Available online at www.sciencedirect.com
ScienceDirect
International Journal of Heat and Fluid Flow 28 (2007) 103–112
International Journal of HEAT AND FLUID FLOW
www.elsevier.com/locate/ijhff

Locally heated shear-driven liquid films in microchannels and minichannels

O.A. Kabov *, Yu.V. Lyulin, I.V. Marchuk, D.V. Zaitsev

Heat Transfer International Research Institute of Universite Libre de Bruxelles and Institute of Thermophysics of Russian Academy of Sciences, Av. Roosevelt 50, B-1050 Brussels, Belgium

Accepted 24 May 2006
Available online 27 September 2006

Abstract

The flow of a locally heated liquid film moving under the friction of gas in a channel is considered through theoretical and numerical modeling and conducting experiments. Theoretical investigation predicts that at $Re_l/Re_g < 0.35$ the main driving force for the film is the friction at the liquid–gas interface. In experiments it was revealed that a liquid film driven by the action of a gas flow in a channel is stable in a wide range of liquid/gas flow rates. A map of isothermal flow regimes was plotted and the lengths of smooth region and region of 2D waves were measured. It was found that the critical heat flux at which an initial stable dry patch forms for a shear-driven liquid film can be several times higher than that for a vertical falling liquid film, which makes shear driven liquid films more suitable for cooling applications. Temperature distribution at the film surface was measured by an infrared scanner and it was found that thermocapillary tangential stresses may exceed tangential stresses caused by the friction of the gas, which indicates a significant Marangoni effect on the film dynamics.

Keywords: Micro/mini channels; Shear-driven liquid film; Local heating; Waves; Film breakdown; Infrared study

1. Introduction

Heated shear-driven liquid films with evaporation are not only a process rich in fundamental physics and hydrodynamics but are also of significant practical importance (Hewitt and Hall-Taylor, 1970; Hanratty, 1991; Aktershev and Alekseenko, 1996; Rosskamp et al., 1998). The film deformations, formation of dry patches as well as heat transfer are governed by viscous, capillary, inertial, and contact-line forces (Ajaev, 2005). Thin annular liquid films may provide very high heat transfer intensity, especially in the micro region near contact-line (Potash and Wayner, 1972; Stephan and Busse, 1992) and may be used for cooling of microelectronic equipment.

The recent development of microelectronics is intimately linked to the problem of thermal regulation. The levels of energy generation in high-speed computer chips are now approaching very high values (up to 100–200 W/cm^2, Schmidt, 2003), and they are on the edge of exceeding the capabilities of today's air-cooling technology. Accordingly, liquid single-phase micro-channel (Kandlikar and Grande, 2004), two-phase flow (Bar-Cohen et al., 1995) and jet-spray (Overholt et al., 2005) direct cooling systems appear to be imperative. On-chip power dissipation is typically not uniform, which limits the total heat dissipation that can be managed by a conventional thermal solution and thus a much more aggressive thermal solution is required (Wang et al., 2005). Using latent heat of vaporization of the fluid to transfer heat efficiently at a nearly constant temperature, micro heat pipes can also be successfully used for cooling electronic devices (Faghri, 1995; Peterson, 1994).

A particularly promising technological solution, allowing to reach high heat fluxes and to decrease space and mass of cooling equipment, is a set-up where heat is transferred to a very thin liquid film driven by a forced gas or vapor flow in

* Corresponding author.
E-mail address: okabov@ulb.ac.be (O.A. Kabov).

0142-727X/$ - see front matter © 2006 Elsevier Inc. All rights reserved.
doi:10.1016/j.ijheatfluidflow.2006.05.010

Nomenclature

B	channel width, m
H	channel height, mm
h	film thickness, mm
h_N	liquid nozzle slot height, mm
g	gravitational acceleration, m/s^2
L	heater length, mm
L_{sm}	length of region of smooth film, mm
L_{br}	length at which 2D waves break, mm
l_σ	scale of capillary-gravitational interaction $= (\sigma/\rho g)^{1/2}$, m
p,P	pressure, Pa
q	heat flux density, W/m^2
q_{idp}	heat flux at which an initial stable dry patch forms, W/m^2
Q	volumetric flow rate, m^3/s
Q_{el}/Q	ratio of evaporated liquid flow rate to initial one, dimensionless
Γ	Specific flow rate $= Q/B$, m^2/s
Re	Reynolds number $= Q\rho/\mu$, dimensionless
T	temperature, °C
u	velocities along axes x, m/s
W_f	width of film flow, mm
$F()$	function
K	ratio between tangential stresses $= \tau_M/\tau_w$, dimensionless

Greek symbols

φ	inclination angle, degree.
ρ	density, kg/m^3
μ	dynamic viscosity, kg/m s
τ	tangential stress on the interface, kg/s^2 m
σ	surface tension coefficient, N/m

Subscripts

0	initial parameters of the flow (at $T = T_0$)
g, l	gas and liquid
s	surface
T, x, y	derivative with respect to T, x, y
w	wall
M	maximum
i, j	number node of x, z

a micro-channel (shear-driven film evaporator, SDFE) (Kabov et al., 2004). Temperature gradients at the gas–liquid interface produce thermocapillary forces, which induce convection and may also lead to the film rupture.

Thermocapillary convection in a liquid film falling down a uniformly or locally heated substrate has been extensively studied during the last decades (see Frank, 2003; Skotheim et al., 2003; Kabov, 1998 and references herein). However, non-uniform heating and Marangoni effects remain only partially understood for shear-driven liquid film flows. The study of these phenomena requires the targeted local measurements and the development of theoretical models aimed to improve the physical understanding of the problem.

2. Theoretical analysis and computation

We consider a channel with rectangular cross section, the height of which, H, is much less than its width B. A layer of viscous incompressible liquid is moving in the channel under the influence of the gas flow as well as under gravity force for a channel inclined at an angle φ with respect to horizontal. A local heat source is embedded into the bottom wall (Fig. 1). It is supposed that the surface tension depends on temperature $\sigma(T) = \sigma_0 - \sigma_T(T - T_0)$ and that σ_0, $\sigma_T = \text{const} > 0$.

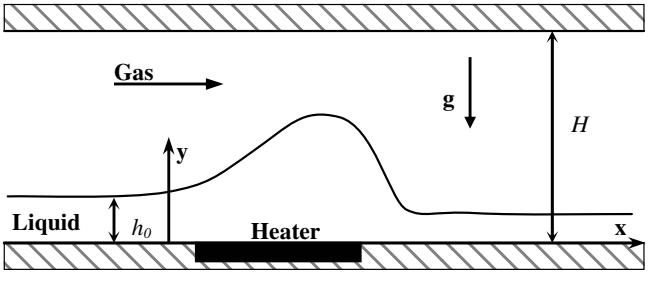

Fig. 1. Sketch of the liquid and gas flow in a microchannel.

Laminar isothermal flow of two layers of incompressible fluids with non-deformable interface is described by simplified Navier–Stokes equations:

$$\mu_l \frac{\partial^2 u_l}{\partial y^2} - \frac{\partial P}{\partial x} = 0, \quad -\frac{\partial P}{\partial y} - \rho_l g = 0, \tag{1}$$

$$\mu_g \frac{\partial^2 u_g}{\partial y^2} - \frac{\partial P}{\partial x} = 0, \quad -\frac{\partial P}{\partial y} - \rho_g g = 0, \tag{2}$$

for liquid film and for gas, respectively. The boundary conditions have the form:

$$u_l|_{y=0} = 0, \quad u_g|_{y=H} = 0 \tag{3}$$

$$u_l \frac{\partial u_l}{\partial y}\bigg|_{y=h} = \mu_g \frac{\partial u_g}{\partial y}\bigg|_{y=h} = \tau, \quad u_g|_{y=h} = u_l|_{y=h}, \tag{4}$$

at the walls and at the gas–liquid interface, respectively. The integration of the first Eq. (1) and first Eq. (2) with boundary conditions (3) and first condition (4) gives equations for liquid and gas velocities:

$$u_l = \frac{1}{\mu_l}\left[\frac{\partial P}{\partial x}\left(\frac{1}{2}y^2 - hy\right) + y\tau\right] \tag{5}$$

$$u_g = \frac{1}{\mu_g}\left[\frac{\partial P}{\partial x}\left(\frac{1}{2}(y^2 - H^2) - h(y - H)\right) + \tau(y - H)\right] \tag{6}$$

Second condition (4) and Eqs. (5) and (6) lead to:

$$\tau = \frac{1}{2}\frac{\partial P}{\partial x}\frac{\mu_g h^2 - \mu_l (h-H)^2}{\mu_g h - \mu_l (h-H)} \tag{7}$$

The conditions of constancy of liquid and gas flow rates yield the formulas:

$$Q_l = \int_0^h \int_0^B u\,dz\,dy = \text{const}, \quad Q_g = \int_h^H \int_0^B u\,dz\,dy = \text{const}, \tag{8}$$

It means that $\partial P/\partial x = \text{const}$. Eqs. 5 and 6 lead to the formulas for specific liquid and gas flow rates:

$$\Gamma_l = \frac{1}{\mu_l}\left[-\frac{h^3}{3}\frac{\partial P}{\partial x} + \tau\frac{h^2}{2}\right] \tag{9}$$

$$\Gamma_g = \frac{1}{\mu_g}\left[\frac{(h-H)^3}{3}\frac{\partial P}{\partial x} - \tau\frac{(h-H)^2}{2}\right] \tag{10}$$

Assigning volumetric flow rates of liquid and gas the pressure drop $\partial P/\partial x$, tangential stress and film thickness may be calculated using Eqs. (7), (9) and (10). The motion of gas is caused by existence of the constant pressure gradient along the channel. The liquid is moving under the influence of two forces, i.e. under pressure gradient and under tangential stress on the gas–liquid interface. A balance of these two forces can be expressed as the ratio $h(\partial P/\partial x)/\tau$. The question arises as which force dominates. Integrating first Eq. (1) leads to:

$$h\partial P/\partial x = \tau - \tau_w, \tag{11}$$

where $\tau_w = \mu_l \partial_{ul}/\partial_y|_{y=0}$. Dividing Eq. (11) by Eq. (7) yields:

$$\frac{\tau_w}{\tau} = 1 + \frac{2\mu_l(H/h-1) + 2\mu_g}{\mu_l(H/h-1)^2 - \mu_g}, \tag{12}$$

The ratio of the shear stresses at the interface and that on the wall is a criterion determining the main driving force. When $\tau/\tau_w > 0.5$ the friction of gas dominates over the pressure gradient. In performed experiments flow rates of gas and liquid provide the ratio of shear stresses $0.39 < \tau/\tau_w < 0.92$ (according to Eq. (12)). However, the majority of experiments (including all those with the heating) are performed at $\tau/\tau_w > 0.5$ so that the friction of gas dominates.

From Eq. (12) it follows that ratio between shear stresses depends on ratio of channel height to film thickness $\tau_w/\tau = F_1(h/H)$. It should be noted that $\lim_{h\to 0} \tau/\tau_w = 1$ and $\lim_{h\to H} \tau/\tau_w = -1$ are asymptotic cases of flow of only gas and liquid, respectively. Dividing Eq. (9) by Eq. (10) and eliminating $\partial P/\partial x$ with the help of Eq. (11), we obtain

$$\frac{\Gamma_l}{\Gamma_g} = \frac{\mu_g\left[\frac{h^2}{3}(\tau_w - \tau) + \tau\frac{h^2}{2}\right]}{\mu_l\left[\frac{(H-h^3)}{3h}(\tau_w - \tau) - \tau\frac{(H-h)^2}{2}\right]}. \tag{13}$$

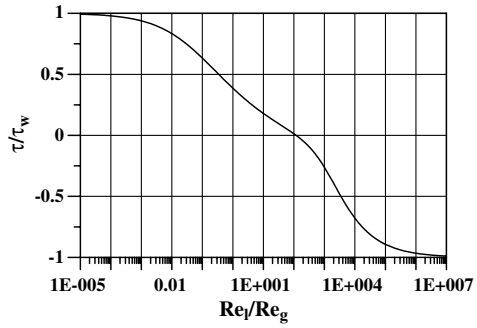

Fig. 2. Ratio between shear stresses versus ratio between Reynolds numbers. H_2O–N_2 flow, calculated using Eq. (12).

Dividing numerator and denominator of the right side of Eq. (13) by $\tau h^2/6$ yields

$$\frac{\Gamma_l}{\Gamma_g} = \frac{\mu_g[2(\tau_w/\tau - 1) + 3]}{\mu_l[2(H/h-1)^3(\tau_w/\tau - 1) - 3(H/h-1)^2]} \tag{14}$$

Since $\tau_w/\tau = F_1(h/H)$ then from (14) it follows that $h/H = F_2(Re_l/Re_g)$ and $\tau_w/\tau = F_3(Re_l/Re_g)$. Thus the ratio between shear stresses and the dimensionless film thickness are functions that depend only on the ratio between Reynolds numbers of liquid and gas, and thus do not depend on the channel height. Fig. 2 represents the dependence of the ratio between shear stresses on the ratio between Reynolds numbers for the flow of water and Nitrogen in a channel at $T = 22$ °C. With increase of Re_l ratio τ/τ_w decreases and contribution of $\partial P/\partial x$ into the liquid flow increases. In performed experiments the ratio Re_l/Re_g varied from 0.002 to 1 (see Fig. 13 below). When the ratio $Re_l/Re_g < 0.35$, the main driving force for the film becomes the friction at the liquid–gas interface. It is important to note that the discussed above calculations are valid if the properties of the liquids are fixed, i.e. for the case of insignificant evaporation.

The non-zero temperature gradient on the film surface leads to appearance of the thermocapillary effects. The theoretical investigation performed in Gatapova et al. (2004) predicts the formation of a liquid bump in the region where thermal boundary layer reaches the film surface, Fig. 3. The positive temperature gradient in the heater area causes the thermocapillary tangential stress directed against the

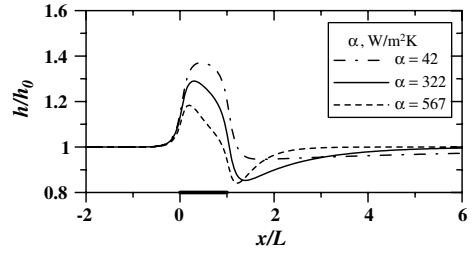

Fig. 3. Film deformation for various heat-transfer coefficients at liquid–gas interface, (Gatapova et al., 2004): FC-72, $T_0 = 17$ °C, $L = 6.7$ mm, $Re_l = 1$, $q = 1000$ W/m^2, $\varphi = 0$, $h_0 = 0.17$ mm, $\tau = 0.024$ kg/s^2 m.

main flow and therefore an increase of the film thickness is observed in the heating area. Downstream of the heater the free surface temperature decreases. The thermocapillary force is directed streamwise in this area, therefore a decrease of the film thickness is observed. This region is most risky for a film breakdown. This theoretical result needs an experimental validation that is out of scope of this paper. It is expected that the bump becomes unstable above a critical value of the imposed heat flux and deforms into streamwise rivulets, similarly to what was demonstrated experimentally (Kabov, 1998) and theoretically (Frank, 2003; Skotheim et al., 2003) for falling liquid films.

It was found in Gatapova et al. (2004) that the damped steady oscillations of free surface upstream the bump may exist if the following inequality is satisfied

$$\tau + \rho g h_0 \sin\varphi > \rho g h_0 \frac{2}{3}\frac{h_0}{l_\sigma}\left(\frac{\cos\varphi}{3}\right)^{3/2} \tag{15}$$

If the film moving forces (shear stress and gravity) overbalance the hydrostatic forces, the damped perturbations of free surface exist. The perturbations always exist when the inclination angle of channel is high ($\varphi \approx 90°$). In the microgravity conditions the damped perturbations of free surface take place at any $\tau > 0$. The damped perturbations are missing in Fig. 3, since the condition (15) is not satisfied (the perturbations are seen in Fig. 4). A trough of up to 5–10% of the initial film thickness was detected upstream of the bump for locally heated falling liquid films (Kabov et al., 2001; Zaitsev et al., 2003) that validate qualitatively the obtained result.

A conjugated 2-D model, based on the long-wave theory, has been proposed in Kabov et al. (2004). Simplified coupled equations for liquid film and gas have been solved analytically. In contrast to the case of infinite flow or large channel height, there is an essential influence of liquid film deformations on pressure and velocity in a gas phase for co-current gas–liquid flow in a microchannel. In Fig. 4 calculations are performed for three cases: (1) gas flow parameters are constant, (2) gas pressure is constant and tangential stress depends on film deformation, (3) gas pressure and tangential stress depend on film deformation. It is shown that the variation of tangential stresses on the interface due to film deformations has a significant effect on the shape of the film. In contrast, gas pressure effect is insignificant. The damped perturbations of free surface upstream the bump exist for all calculations.

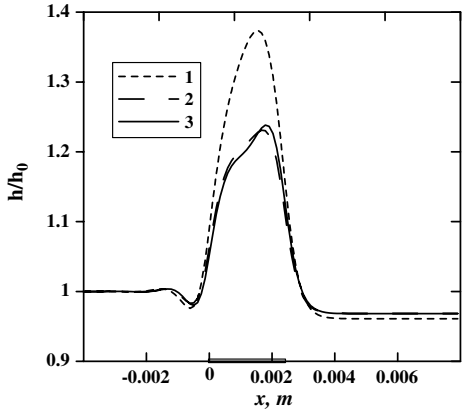

Fig. 4. Film deformation, (Kabov et al., 2004): FC-72, $T_0 = 20$ °C, $L = 2.5$ mm, $h_0 = 50$ μm, $H = 150$ μm, $q = 0.5$ W/cm^2, $u_{g0} = 1.8$ m/s, $Re_l = 2.705$. (1) $-\tau = \text{const}$, $p_g = \text{const}$; (2) $-\tau = \tau(u)$, $p_g = \text{const}$ and (3) $-\tau = \tau(u)$, $p_g = p_g(u)$.

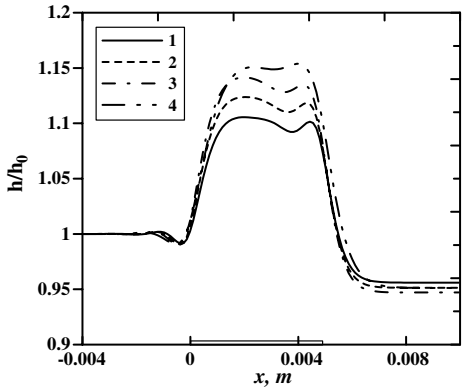

Fig. 5. Channel height effect on film deformation, (Kabov et al., 2004): FC-72, $T_0 = 20$ °C, $L = 5$ mm, $h_0 = 60$ μm, $q = 0.75$ W/cm^2, $u_{g0} = 2.5$ m/s. 1—$H = 160$ μm; 2—$H = 240$ μm; 3—$H = 500$ μm; 4—$H =$ infinity.

Gas velocity increases with increase of film thickness deformation and this effect is more pronounced for small channel height, Fig. 5. Increasing of tangential stresses on the interface caused by the gas flow decreases the film thickness. Calculations are performed for FC-72 highly subcooled up to the saturation temperature (56 °C at atmospheric pressure) and relatively small feat fluxes ($T_s < 55$ °C), because evaporation has not been taken into account. More detailed experiments with greater accuracy of measurements or more precise numerical calculations are needed to verify these results.

The evaporation effect on heat transfer from a local heat source to a liquid film moving by a gas flow has been studied by the authors of Gatapova et al. (2005) in the framework of 2-D model. Using Eqs. (5) and (6) for liquid and gas velocities the joint solution of heat transfer and diffusion problem with corresponding boundary condition was studied. It was assumed that total mass flow rate of evaporated liquid is much less than total mass flow rate of liquid film, and that evaporated substance is an impurity of small concentration in gas, scarcely affecting gas thermodynamic properties. The film temperature is reducing more rapidly, when evaporation process takes place, Fig. 6. There is a practically linear increase of temperature in the heater area, Fig. 7. The influence of convective heat transfer mechanism is becoming stronger with increasing Re_l. The length of the thermal boundary layer also increases with increasing Re_l. The temperature reduction downstream of the heater is explained by evaporation and convective heat transfer between surface of the film and gas flow. In Fig. 7 flow regimes with Re equal to 0.5 and 5 correspond to film thickness equal to 84 μm and 210 μm, respectively.

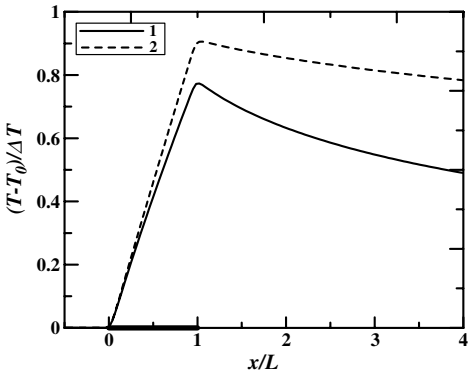

Fig. 6. Temperature on H_2O–N_2 interface, (Gatapova et al., 2005): 1—including evaporation, $Q_{el}/Q = 0.039$, 2—without evaporation. $T_0 = 17$ °C, $q = 0.1$ W/cm^2, $\varphi = 0$, $H = 1$ mm, $L = 2$ mm, $Re_l = 0.5$, $Re_g = 80$.

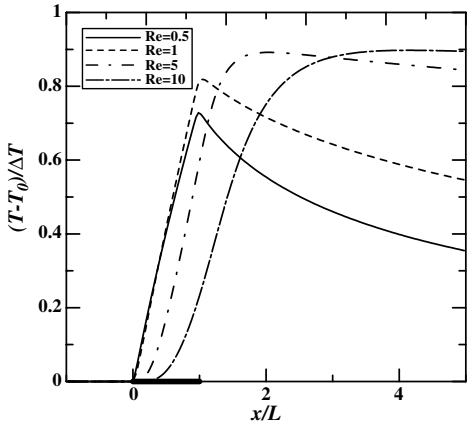

Fig. 7. Liquid Re number effect on temperature on H_2O–N_2 interface, (Gatapova et al., 2005): $T_0 = 17$ °C, $q = 10$ W/cm^2, $\varphi = 0$, $H = 1$ mm, $L = 2$ mm, $Re_g = 200$.

3. Experimental setup

Schematic of experimental setup is presented in Fig. 8. Fig. 9 shows design of test section. The main part of the

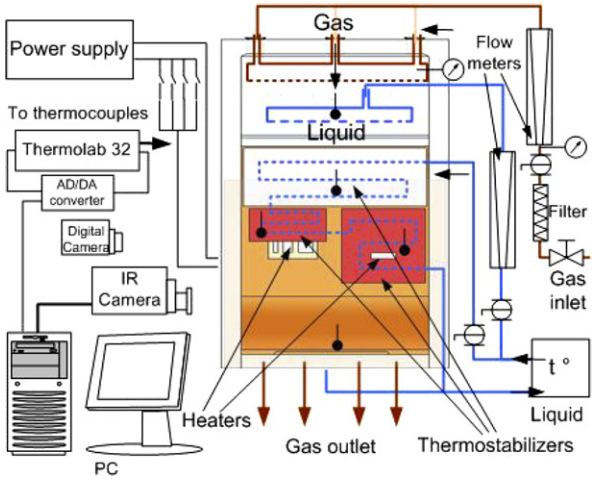

Fig. 8. Schematic of experimental setup.

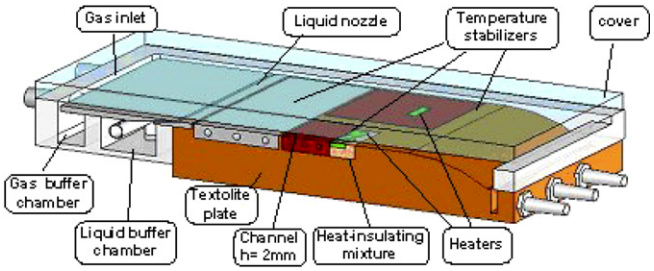

Fig. 9. Design of test section.

test section is a plate made of textolite (resin impregnated fabric laminate) having dimensions of $250 \times 195 \times 40$ mm in length, width and depth, respectively. The plate is covered with a transparent, plexiglass cover so that a channel of variable height $H = 1$–3 mm can be created. Gas is supplied from a compressor into the gas buffer chamber fixed at the top of the textolite plate. The gas enters the channel through a 2 mm slot and passes to the atmosphere at the bottom part of the test section. The liquid is pumped into the liquid buffer chamber from a thermostat which keeps the liquid at a constant temperature T_{0l}. The film, formed by the nozzle of variable height $h_N = 0.15$–0.25 mm, is driven in the channel by the shear stress of gas. The liquid is accumulating at the bottom part of the test section and is returned into the thermostat. Distance from the gas inlet to the liquid nozzle is 85 mm, which provides steady flow of gas at the moment it reaches the film. Distance from the liquid nozzle to the heaters # 1–3 is 113 mm, to the heater # 4 is 124 mm.

The test section contains four electrical heaters with different dimensions. Three of them, sized 4×11, 6.5×11 and 13×11 mm, are embedded into the textolite plate. Upstream of the heaters a copper block with a system of internal channels is situated through which working liquid with temperature T_{0l} is pumped. This ensures the temperature of the film, flowing onto the heaters, to be constant. The fourth heater of 22×6.55 mm size is embedded separately into another thermostabilizing copper block (Figs. 9 and 10). The base of each heater is a stainless steel plate with thickness of 3.95 mm, to the inner surface of which a flat resistor is attached (Fig. 11). Each heater allows obtaining the local heat flux at several points via the temperature drop measurement across the stainless steel plate with the help of thermocouples. In order to minimize heat spreading from the heaters, a gap around the heaters is

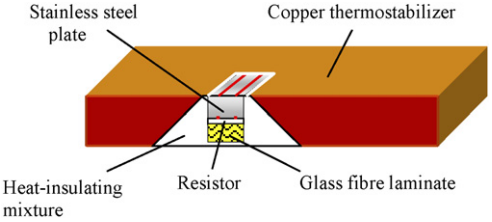

Fig. 10. Design of the substrate.

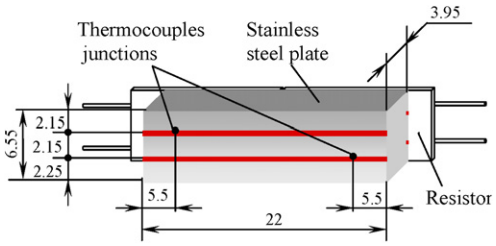

Fig. 11. Design of the fourth heater.

filled with a mixture of epoxy resin and charcoal. Thermal conductivity of the mixture is 0.15 W/mK that is 100 times lower than that of the stainless steel. The gap around the fourth heater is 1 mm wide at the level of working surface.

In the present experiments the test section is set horizontally. Water and air are used as the working liquid and gas, respectively. Experiments are carried out at atmospheric pressure and $T_{0l} = 20$–22 °C. Initial temperature of the gas $T_{0g} = 22$–25 °C coincides with ambient temperature. Channel height is 2 mm. Some experiments are performed on the full wide channel with the width of the liquid film flow of $W_f = 120$ mm. However, most of the experiments (including all those with the heating) are performed on reduced channel with $W_f = 65$ mm, which provides more stable film flow.

Control of uniformity of the gas flow in spanwise direction was performed with the help of a steel capillary of external diameter 0.7 mm which was inserted into the channel at the distance of 78 mm from gas inlet, and directed opposite to the flow. The capillary was connected to a micromanometer. Fig. 12 shows distribution of the dynamic pressure in the channel for different gas flow rates. Uniformity of the dynamic pressure in spanwise direction is within ±4% at $Re_g = 1400$ and ±20% at $Re_g = 800$. Since flow rate is proportional to the square root of the dynamic pressure, one can conclude that uniformity of the gas flow rate is within ±2–10%.

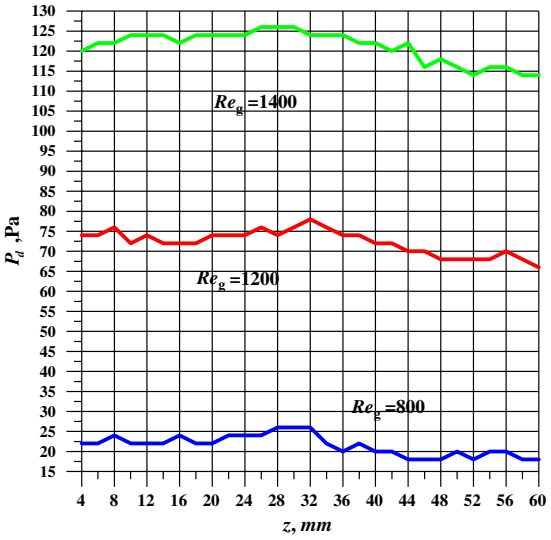

Fig. 12. Uniformity of gas flow in the minichannel.

4. Isothermal flow of liquid film

Isothermal flow (all heaters switched off) was investigated in the range of $Re_l = 1$–60 and $Re_g = 60$–1950. Fig. 13 shows the obtained flow regime map. For $W_f = 65$ mm the film flow is considerably more stable against breakdown than for $W_f = 120$ mm. The film flow is also somewhat more stable for lower h_N (data 1, 2 versus data 3). At relatively high Re_l and relatively small Re_g the film thickness is so high resulting in channel flooding.

For small liquid and gas flow rates the film surface is smooth. With increasing Re_l and Re_g, first two-dimensional

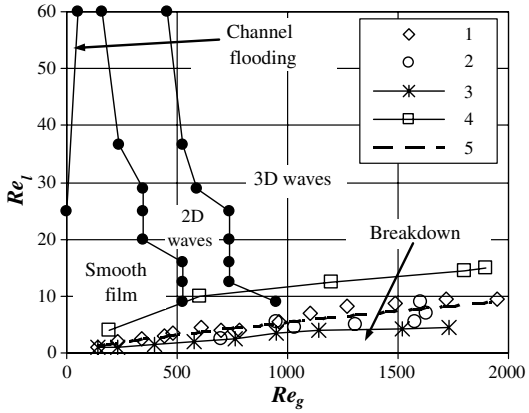

Fig. 13. Map of isothermal flow regimes. Breakdown: 1—$W_f = 65$ mm, $h_N = 250$ μm, run 1; 2—$W_f = 65$ mm, $H_N = 250$ μm, run 2; 3—$W_f = 65$ mm, $H_N = 150$ μm; 4—$W_f = 120$ mm, $H_N = 200$ μm; 5—generalization of data 1 and 2. All the rest data—$W_f = 65$ mm, $h_N = 200$ μm.

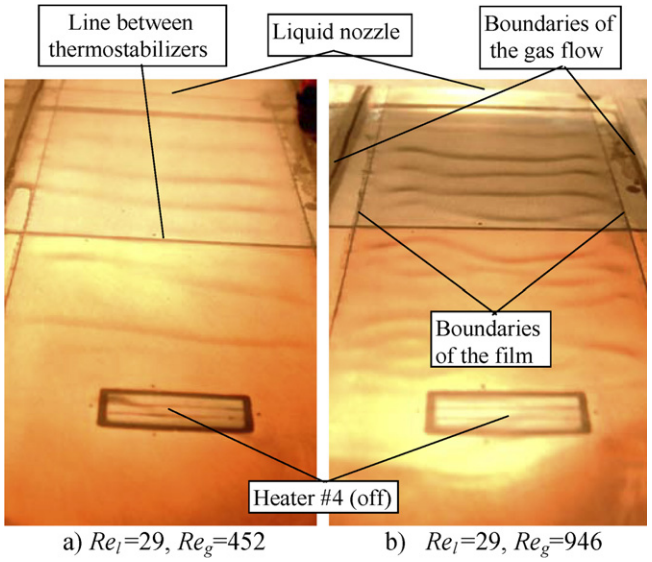

Fig. 14. Photographs of two-dimensional (a) and three-dimensional (b) waves, $W_f = 65$ mm, $h_N = 200$ μm.

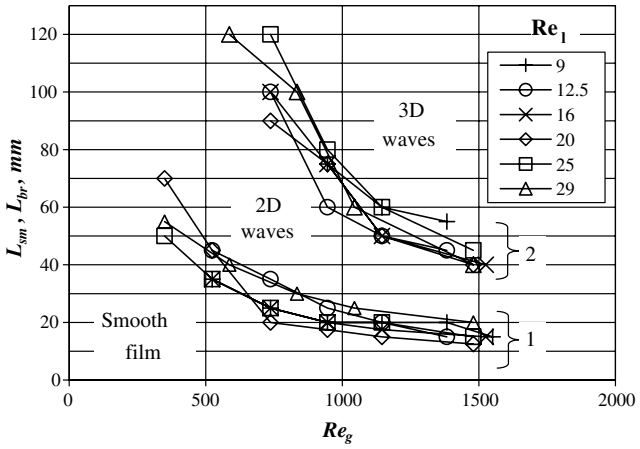

Fig. 15. Length of smooth region (1) and length of region of 2D waves (2) depending on Re_l and Re_g, $W_f = 65$ mm, $h_N = 200$ μm.

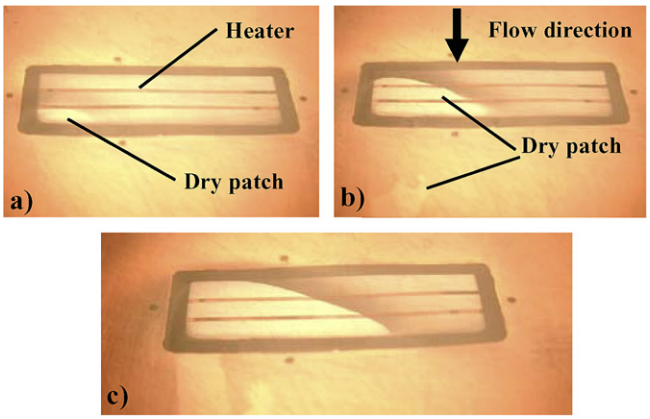

Fig. 16. Dynamics of dry patch formation, $Re_l = 16$, $Re_g = 524$, $q = 4$ W/cm^2. Pictures are taken with interval of about 15 s.

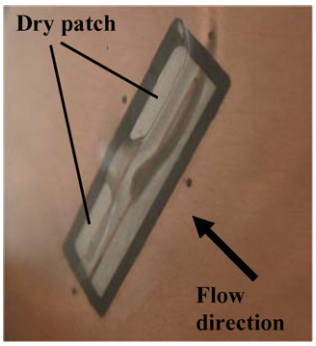

Fig. 17. 3D deformations with dry patches, $Re_l = 20$, $Re_g = 946$, $q = 9.1$ W/cm^2.

(2D) waves form at the film surface and then they break into three-dimensional (3D) ones. Fig. 14 shows photographs of the flow. Influence of Re_l and Re_g on the length of the smooth film, L_{sm}, and length at which 2D waves break, L_{br}, is shown in Fig. 15. One can see that L_{sm} as well as L_{br} decrease with increasing Re_g, while being practically independent on Re_l. Waves were detected by visual observations. Statistical error in determining L_{sm} and L_{br} was about ±10 mm.

5. Breakdown of locally heated film

Liquid film breakdown was investigated using the fourth heater (22×6.55 mm) in the range of the average heat flux $q = 0.87$–32.1 W/cm^2, which was determined by the electric power dissipated on the heater. Parameters of the experiment: $Re_l = 5.5$–36.5, $Re_g = 160$–1480, $W_f = 65$ mm, $h_N = 200$ μm. The scenario of film breakdown is different for different flow regimes. In the regime of smooth film (see Fig. 13), the increase of the heat flux first causes a faintly visible deformation of the film surface at the bottom edge of the heater and then the film suddenly breaks down, with virtually instant dryout of the whole heating area.

In the regime of 2D waves, breakdown is preceded by formation in the film of an unstable hollow at the bottom part of the heater, periodically enhanced by the passage of 2D waves. The first stable dry patch forms at some critical heat flux at the bottom edge of the heater and slowly increases in size with time as depicted in Fig. 16. With further increase of the heat flux it covers the entire heater. In the regime of 3D waves, the increase of the heat flux leads to formation of an unstable 3D structure, heavily altered by the passing 3D waves. With increase of the heat flux, usually two dry patches form at the bottom edge of the heater, making the 3D structure more stable, Fig. 17. This structure resembles the so called "regular structures" (a rivulet structure wavelike in spanwise direction) forming in a gravitationally falling smooth ($Re < 10$) liquid film under local heating (Kabov, 1998).

Common to all of the film flow regimes is initiation of dry patches from the bottom edge of the heater. The theoretical research also predicts that this region is most risky for the breakdown (see Fig. 3). It is worth noting that in case of a locally heated gravitational liquid film, dry patches usually form at the upper edge of the heater and spread downstream (Kabov, 2000). One possible reason is that in Kabov (2000) there was no temperature stabilizer around the heater and thus no significant temperature gradient was achieved in the region of the bottom edge of the heater (see Figs. 20 and 21 below). Another distinguishing feature of breakdown of a gravitational liquid film is that the first dry patch formed is normally stable, while for a shear-driven liquid film first dry patches are often unstable (being periodically washed out), with the initial stable dry patch forming at the heat flux of up to 20% higher (this is more pronounced for higher gas flow rates). This is probably because in case of a shear-driven liquid film, dry patches are washed out by the intense waves and also are "blown" away by the gas flow.

Fig. 18 shows the critical heat flux at which an initial stable dry patch forms, q_{idp} depending on Re_l and Re_g. It is seen that q_{idp} increases with increasing both Re_l and Re_g. Dashed line represents previously obtained data on breakdown of a gravitational water film falling down a

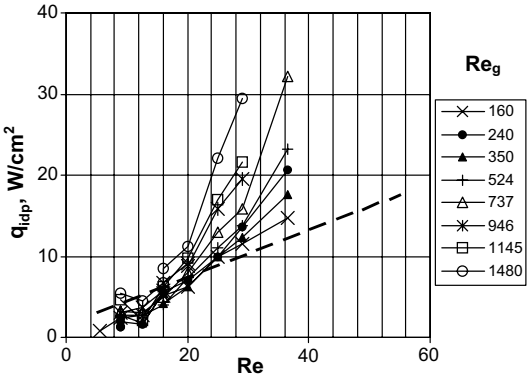

Fig. 18. The critical heat flux for film breakdown depending on Re_l and Re_g, dashed line—data on a falling water film (Kabov, 2000).

vertical plate with a heater of 13×6.5 mm (similar length) (Kabov, 2000). At relatively small Re_l the shear-driven liquid film breaks down at similar or even lower heat fluxes compared to gravitational one. However at higher liquid Re number q_{idp} for shear-driven liquid film is up to three times higher. Use of higher gas flow rates will probably allow to reach even higher values of q_{idp} for a fixed liquid Re number. This makes use of shear-driven liquid films in cooling systems very promising.

6. IR study of film flow

Temperature distribution at the film surface is measured by an infrared (IR) scanner which perceives IR emission in the range of wavelength $3.5 \div 5.5$ μm. Radiation from the film passes through a 50×65 mm window made of polypropylene film, inserted into the cover, Fig. 10, then reflects from a mirror and arrives to the lens of the IR scanner. The frame is 192×192 pixels having dimensions at the film surface from 68×62 to 72×68 mm. Scanning time is 2.5 s per frame. Maximum sensitivity of the scanner, in terms of temperature difference, is 0.06 °C (equal to the signal noise at 30 °C).

Conversion of measured IR radiation intensity to the temperature is performed via measuring radiation intensity from the initial film and from a calibrated irradiator. Emission coefficient of liquid and that of the irradiator are different, therefore at a given temperature the film and the irradiator result in different measured IR radiation intensities. During a calibration the dependence was obtained between the temperature of the film surface and that of the irradiator at the same intensity of accepted radiation.

Fig. 19 represents IR images of the film for different flow regimes. The heater is indicated with a black frame. When the film is smooth, the temperature distribution is quasi-stationary, which is confirmed by the fact that single-frame and averaged thermograms are practically identical. That is not the case for wavy film. Heat flux effect on streamwise temperature distribution at the film surface is shown in Fig. 20. Figs. 19–21 show that there is a non-uniform span-

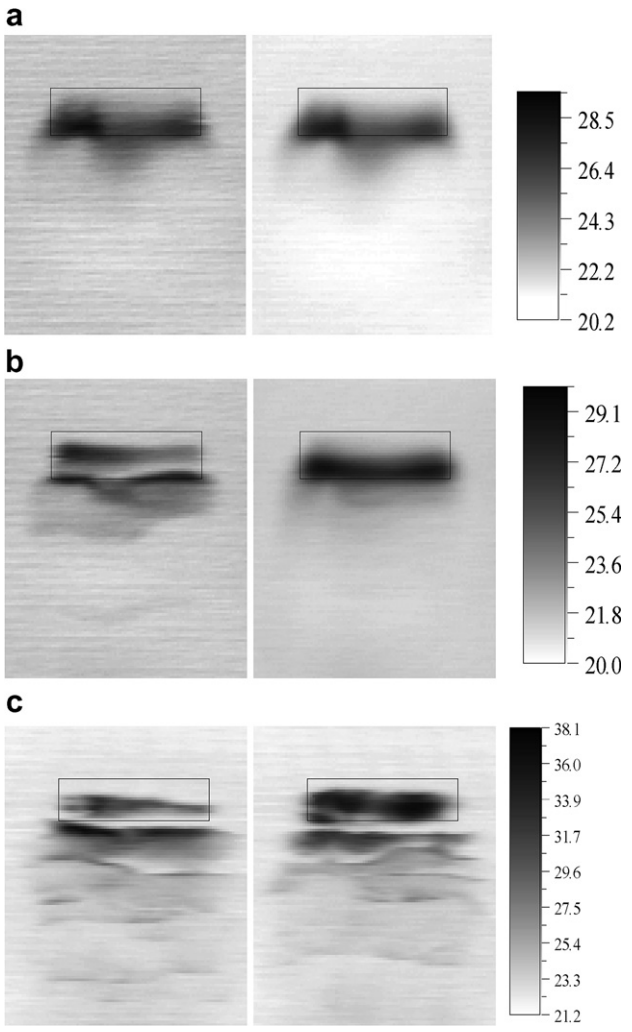

Fig. 19. Images of film surface temperature. Left image is single frame; right image is averaging over 10 frames. (a) $Re_l = 8.5$, $Re_g = 534$, $q = 3.8$ W/cm^2, smooth film, $\tau = 0.273$ Pa, $\tau_w = 0.341$ Pa, $\tau/\tau_w = 0.8$, (b) $Re_l = 12.4$, $Re_g = 620$, $q = 4.47$ W/cm^2, 2D waves, $\tau = 0.324$ Pa, $\tau_w = 0.414$ Pa, $\tau/\tau_w = 0.78$ and (c) $Re_l = 32$, $Re_g = 1164$, $q = 14.36$ W/cm^2, 3D waves, $\tau = 0.632$ Pa, $\tau_w = 0.834$ Pa, $\tau/\tau_w = 0.76$.

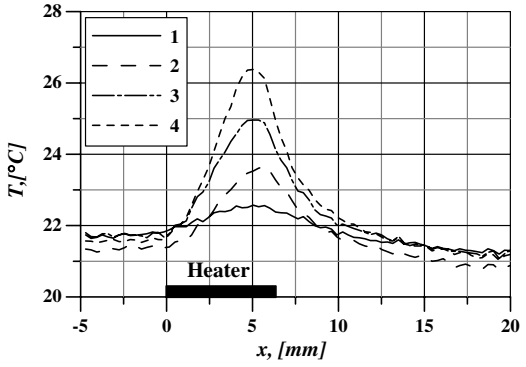

Fig. 20. Temperature at the film surface averaged on the heater width, $Re_l = 8.5$, $Re_g = 534$, 1—$q = 1.01$ W/cm^2, 2—1.88 W/cm^2, 3—3.04 W/cm^2, 4—3.8 W/cm^2.

wise temperature distribution and that the maximum of the surface temperature is located upstream the bottom edge of

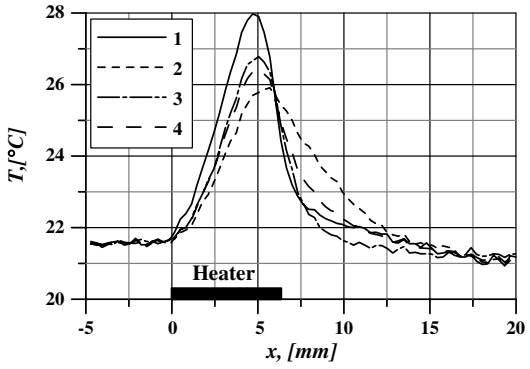

Fig. 21. Temperature at the film surface, $Re_l = 8.5$, $Re_g = 534$, $q = 3.8$ W/cm^2: 1—at the center of the left part of the heater, 2—at the center of the heater, 3—at the center of the right part of the heater, 4—averaged on the heater width.

the heater. This fact may be attributed to the 3D film deformation because of the Marangoni effect. More detailed experiments with greater accuracy of measurements are needed to verify these results.

The liquid film surface is susceptible to two kinds of tangential stress: one is caused by the friction of the gas the other is caused by the temperature gradient at the film surface $\tau_M = \sigma_T|\mathrm{grad}(T)|_{MAX}$. Thermocapillary tangential stress can be aligned with the main flow (at the downstream part of the heater) as well as opposite to the flow (at the upstream part of the heater). The temperature gradient field is calculated by the difference method. As the components of local gradient vector at a point (i,j) central differences are taken

$$\partial T(i,j)/\partial x = [T(i,j-1) - T(i,j+1)]/2h_x \quad (16)$$

$$\partial T(i,j)/\partial z = [T(i-1,j) - T(i+1,j)]/2h_z \quad (17)$$

For the frame with 70×65 mm size the distance between measuring points at the film surface is $h_z = 0.36$ mm in spanwise direction and $h_x = 0.34$ mm in streamwise direction. Absolute value of the local temperature gradient is calculated as a length of the vector

$$|\mathrm{grad}\, T| = ((\partial T/\partial x)^2 + (\partial T/\partial z)^2)^{1/2} \quad (18)$$

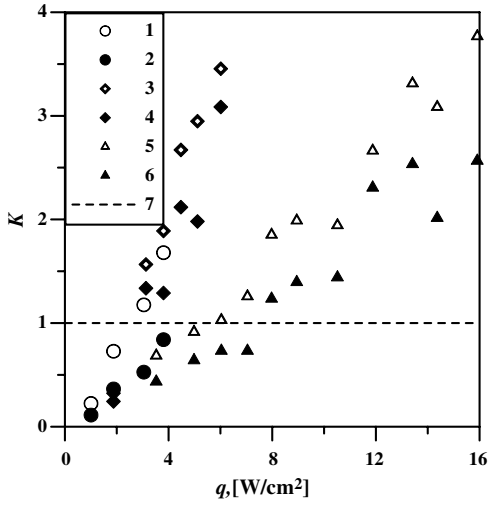

Fig. 22. Ratio of measured thermocapillary tangential stress to tangential stress at the wall calculated for non-deformed film: 1,2—$Re_l = 8.5$, $Re_g = 534$; 3,4—$Re_l = 12.4$, $Re_g = 620$; 5,6—$Re_l = 32$, $Re_g = 1164$.

Fig. 22 shows the ratio between tangential stresses $K = \tau_M/\tau_w$, where τ_M is measured thermocapillary tangential stress, τ_w is shear stress on the wall calculated using Eq. (11). White symbols represent data calculated on maximal temperature gradients, and averaged over 10 frames. Black symbols represent data calculated on maximal temperature gradients, and averaged over the heater width and over 10 frames. It is seen that at sufficiently high heat fluxes ratio K begins to exceed unit.

7. Conclusions

The paper focuses upon shear-driven liquid film evaporative cooling of high-speed computer chips. The recent progress that has been achieved through conducting theoretical and numerical modeling as well as new experimental data has been discussed. Thin liquid films may provide very high heat transfer intensity, however development of cooling system based on thin film technology requires significant advances in fundamental research, since the stability of joint flow of locally heated liquid film and gas is rather complex problem and rupture of the film may occur.

An analytical solution of the problem in case of steady two-dimensional isothermal flow of a non-deformable laminar film and gas in a horizontally oriented channel was obtained. It was found that at $Re_l/Re_g < 0.35$ the main driving force for the film is the friction at the liquid–gas interface.

A new experimental setup that contains a mini-channel with transparent wall and several flash-mounted electrical heaters was created. Heating element with dimensions of 22×6.55 mm^2 was used in the experiments. Experiments showed that a liquid film driven by the action of a gas flow in a channel is stable in a wide range of liquid/gas flow rates. A map of isothermal flow regimes was plotted and the lengths of smooth region and region of 2D waves were measured.

Breakdown of a locally heated liquid film shear-driven in a channel was investigated and it was found that scenario of film breakdown differs widely for different flow regimes. It was revealed that the critical heat flux at which an initial stable dry patch forms is up to three times higher than that for a vertical falling liquid film, which makes shear driven liquid films more suitable for cooling applications.

Temperature distribution at the film surface is measured by an infrared scanner and it was shown that thermocapillary tangential stresses may exceed tangential stresses caused by the friction of the gas, which indicate a significant Marangoni effect on film dynamics.

Acknowledgements

The authors gratefully acknowledge support of this work by the Russian Foundation for Basic Research (Project # 05-08-65426) as well as by the Human Capital Foundation and by ESA in the framework of MAP "Boiling" Project. Z.D.V. acknowledges support of INTAS Grant No. 03-55-1791, Lavrentiev's young scientist grant and also grant of President of Russian Federation No. MK-3651.2005.8. L.Y.V. acknowledges support of INTAS Grant No. 04-83-2952.

References

Ajaev, V.S., 2005. Spreading of thin volatile liquid droplets on uniformly heated surfaces. J. Fluid Mech. 528, 279–296.

Aktershev, S.P., Alekseenko, S.V., 1996. Interfacial instabilities in an annular two-phase flow. Russ. J. Eng. Thermophys. 6 (4), 307–320.

Bar-Cohen, A., Sherwood, G., Hodes, M., Solbreken, G.L., 1995. Gas-assisted evaporative cooling of high density electronic modules. IEEE Trans. CPMT A 18 (3), 502–509.

Faghri, A., 1995. Heat Pipe Science and Technology. Taylor and Francis, Washington.

Frank, A.M., 2003. 3D numerical simulation of regular structure formation in a locally heated falling film. Eur. J. Mech. B/Fluids 22, 445–471.

Gatapova, E.Ya., Kuznetsov, V.V., Kabov, O.A., Legros, J.-C., 2005. Annular liquid film flow under local heating in microchannels. In: Proc. III Int. Conf. on Microchannels and Minichannels, Toronto, Paper ICMM2005-75253.

Gatapova, E.Ya., Marchuk, I.V., Kabov, O.A., 2004. Heat transfer and two-dimensional deformations in locally heated liquid film with co-current gas flow. J. Thermal Sci. Eng. The Heat Transfer Society of Japan 12 (1), 27–34.

Hewitt, G.F., Hall-Taylor, M.S., 1970. Annular Two-phase Flow. Pergamon Press, Oxford.

Hanratty, T.J., 1991. Separated flow modeling and interfacial transport phenomena. Appl. Sci. Res. 48, 353–390.

Kandlikar, S.G., Grande, W.J., 2004. Evaluation of single phase flow in microchannels for high flux chip cooling – thermohydraulic performance enhancement and fabrication technology. In: Proc. II Int. Conf. on Microchannels and Minichannels, pp. 67–76.

Kabov, O.A., Kuznetsov, V.V., Legros, J.-C., 2004. Heat transfer and film dynamic in shear-driven liquid film cooling system of microelectronic equipment. In: Proc. II Int. Conf. on Microchannels and Minichannels, Rochester, pp. 687–694.

Kabov, O.A., 1998. Formation of regular structures in a falling liquid film upon local heating. Thermophys. Aeromech. 5 (1), 547–551.

Kabov, O.A., Legros, J.C., Marchuk, I.V., Scheid, B., 2001. Deformation of the free surface in a moving locally-heated thin liquid layer. Fluid Dyn. 36 (3), 521–528.

Kabov, O.A., 2000. Breakdown of a liquid film flowing over the surface with a local heat source. Thermophys. Aeromech. 7 (4), 513–520.

Overholt, M.R., McCandless, A., Kelly, K.W., Becnel, C.J., Motakef, S., 2005. Micro-jet arrays for cooling of electronic equipment, In: Proc. III Int. Conf. on Microchannels and Minichannels, Toronto, Paper ICMM2005-75250.

Peterson, G.P., 1994. An introduction to heat pipesModeling, Testing and Applications. John Wiley and Sons.

Potash, M., Wayner, P.C., 1972. Evaporation from a two-dimensional extended meniscus. Int. J. Heat Mass Transfer 15, 1851–1863.

Rosskamp, H., Willmann, M., Wittig, S., 1998. Heat up and evaporation of shear driven liquid wall films in hot turbulent air flow. Int. J. Heat Fluid Flow 19, 167–172.

Stephan, P., Busse, C.A., 1992. Analysis of heat transfer coefficient of grooved heat pipe evaporator walls. Int. J. Heat Mass Transfer 35, 383–391.

Schmidt, R., 2003. Challenges in electronic cooling – opportunities for enhanced thermal management techniques – microprocessor liquid cooled minichannel heat sink. In: Proc. I Int. Conf. on Microchannels and Minichannels, Rochester, pp. 951–959.

Skotheim, J.M., Thiele, U., Scheid, B., 2003. On the instability of a falling film due to localized heating. J. Fluid Mech. 475, 1–19.

Wang, P., Bar-Cohen, A., Yang, B., Solbreken, G.L., Zhang, Y., Shakouri, A., 2005. thermoelectric micro-cooler for hot-spot thermal management. In: Proc. InterPACK'05: Tech. Conf. and Exhibition on Integration and Packaging of MEMS, NMES and Electronic Systems, San Francisco, Paper IPACK2005-73244.

Zaitsev, D.V., Kabov, O.A., Evseev, A.R., 2003. Measurement of locally heated liquid film thickness by a double-fiber optical probe. Exp. Fluids 34, 748–754.